Environmental Research Letters

LETTER

Drought-induced regime shift and resilience of a Sahelian ecohydrosystem

Valentin Wendling[1], **Christophe Peugeot**[1,6], **Angeles G Mayor**[2], **Pierre Hiernaux**[3], **Eric Mougin**[3], **Manuela Grippa**[3], **Laurent Kergoat**[3], **Romain Walcker**[4], **Sylvie Galle**[5] and **Thierry Lebel**[5]

[1] Hydrosciences Montpellier (HSM), IRD, Univ. Montpellier, CNRS, Montpellier, France
[2] Copernicus Institute of Sustainable Development Géosciences Environnement, Utrecht Univ., Utrecht, Netherlands
[3] Géosciences Environnement Toulouse (GET), CNRS, IRD, UPS, Toulouse, France
[4] Laboratoire écologie fonctionnelle et environnement (ECOLAB), UPS, CNRS, Toulouse-INP, Toulouse, France
[5] Univ. Grenoble Alpes, CNRS, IRD, Grenoble INP, UMR IGE, Grenoble, France
[6] Author to whom any correspondence should be addressed.

E-mail: valentin.wendling@ird.fr, christophe.peugeot@ird.fr, A.GarciaMayor@uu.nl, pierre.hiernaux2@orange.fr, mouginbassignac@aol.com, manuela.grippa@get.omp.eu, laurent.kergoat@get.omp.eu, romain.walcker@univ-tlse3.fr, sylvie.galle@ird.fr and thierry.lebel@univ-grenoble-alpes.fr

OPEN ACCESS

RECEIVED
28 March 2019

REVISED
9 August 2019

ACCEPTED FOR PUBLICATION
22 August 2019

PUBLISHED
4 October 2019

Keywords: Sahel, eco-hydrology, alternative stable states, regime shifts, rainfall variability

Supplementary material for this article is available online

Abstract

The Sahel (a semi-arid fringe south of the Sahara) experienced a long and prolonged drought from the 1970s to the mid-1990s, with a few extremely severe episodes that strongly affected ecosystems and societies. Long-term observations showed that surface runoff increased during this period, despite the rainfall deficit. This paradox stems from the soil degradation that was induced by various factors, either directly linked to the drought (impact on vegetation cover), or, in places, to human practices (land clearing and cropping). Surface runoff is still increasing throughout the region, suggesting that Sahelian ecohydrosystems may have shifted to a new hydrological regime. In order to explore this issue, we have developed a simple system dynamics model incorporating vegetation–hydrology interactions and representing in a lumped way the first order processes occurring at the hillslope scale and the annual timestep. Long term observations on a pilot site in northern Mali were used to constrain the model and define an ensemble of plausible simulations. The model successfully reproduced the vegetation collapse and the runoff increase observed over the last 60 years. Our results confirmed that the system presents two alternative states and that during the drought it shifted from a high-vegetation/low-runoff regime to the alternative low-vegetation/high-runoff one, where it has remained trapped until now. We showed that the mean annual rainfall deficit was sufficient to explain the shift. According to the model, vegetation recovery and runoff reduction are possible in this system, but the conditions in which they could occur remain uncertain as the model was only constrained by observations over the collapse trajectory. The study shows that the system is also sensitive to the interannual and decadal variability of rainfall, and that larger variability leads to higher runoff. Both mean rainfall and rainfall variability may increase in central Sahel under climate change, leading to antagonist effects on the system, which makes its resilience uncertain.

1. Introduction

Due to interactions between changing external forcing factors (e.g. rainfall) and internal dynamics, an environmental system (e.g. a forest) may shift into new states where it stays even if the forcing factors return to their initial value. In such a system, two alternative stable states may exist towards which the system is attracted (e.g. forest versus savannah, Staver *et al* 2011). For certain conditions, both equilibria can coexist and the system can shift abruptly from one to the other when critical thresholds (or tipping points)

are passed (review in Scheffer *et al* 2001). This kind of behaviour has been widely studied in ecological systems (Scheffer and Carpenter 2003, Rietkerk *et al* 2004, Hirota *et al* 2011, van Nes *et al* 2014, Yin *et al* 2014), among others. Attention has been also paid to regime shifts in human societies driven by environmental factors (Di Baldassarre *et al* 2013, Broderstad and Eythorsson 2014, Sivapalan 2015, Downey *et al* 2016, Kuil *et al* 2016).

Global change might increase the potential for the tipping of some key elements of the Earth's system (Lenton *et al* 2008, Barnosky *et al* 2012, Steffen *et al* 2018). Whilst the existence of tipping points at the planetary scale (Brook *et al* 2013) and their propagation across scales (Hughes *et al* 2013) is debated, examples exist at the regional scale, such as the the collapse of the 'green Sahara' and the shrinking of Lake Chad around 6000 BP as a response to a gradual change in the Earth's orbital parameters (Claussen *et al* 1999).

Marked and persistent ecohydrological changes have been observed in the Sahel (a semi-arid belt south of the Sahara) over the past 60 years. This region experienced a severe and prolonged drought from the 1970s onwards (Lebel and Ali 2009), with extremely severe episodes that have strongly and durably affected ecosystems and societies. Over most of the Sahel, greening has been observed by satellite imagery since the 1980s (Fensholt *et al* 2012, Dardel *et al* 2014). Concurrently, long-term observations have shown that the outflow of Sahelian watersheds has increased from the 1950s onwards (Mahé and Paturel 2009, Gardelle *et al* 2010, Descroix *et al* 2012, Gal *et al* 2016), including during the drought (the so-called 'Sahelian paradox'; Favreau *et al* 2009). Field studies showed that these apparently conflicting changes resulted from smaller scale, soil-dependent, processes. Vegetation (mainly herbaceous) recovered on deep sandy soils, driven by post-drought rainfall increase, whereas it decayed on shallow soils, despite the annual rainfall trend, causing erosion and runoff (Dardel *et al* 2014, Trichon *et al* 2018, Gal *et al* 2017). In some highly populated areas (e.g. South West Niger), this so-called regreening was not observed due to the impact of human activities (land clearing, crops which are less green than rangelands, fertility losses; Favreau *et al* (2009), Hiernaux *et al* (2009).

As in other semi-arid regions, the Sahelian hydrology is strongly dependent on surface conditions (e.g. Casenave and Valentin 1992, Peugeot *et al* 1997). At the elementary scale, heavy rains favour soil crusting all the more since the vegetation cover is sparse; a loss (gain) of vegetation cover favours (prevents) erosion and fertility losses, which in turn prevents (favours) vegetation expansion. These small-scale mechanisms combine into a positive feedback loop which has been shown to be involved in larger scale desertification dynamics (D'Odorico *et al* 2013, Wilcox *et al* 2017, Saco *et al* 2018). If the feedback is strong enough, catastrophic transitions between the alternative low and high runoff states (and the corresponding high and low vegetation ones) can occur (Mayor *et al* 2013, Kefi *et al* 2016). The observed ecohydrological changes on the scale of the whole Sahel show some similarities with these small-scale mechanisms. They suggest that the 1970–1994 drought could have triggered a shift to a high runoff state at the elementary scale, which would have resulted in the new hydrological regime observed at the regional scale.

The outflow of Sahelian watersheds has continued to increase in recent years (Descroix *et al* 2018), which is associated with an intensification of rainfall (Taylor *et al* 2017, Panthou *et al* 2018) and floods (Wilcox *et al* 2018, Tamagnone *et al* 2019), and these trends are expected to persist with climate change (Giannini *et al* 2013, Monerie *et al* 2017, Martin 2018). Land conversion to croplands is also expected to continue over the coming decades as a result of one of the highest population growths worldwide (UN 2017). How these changes will impact future water resources and living conditions is still largely unknown. In particular, the possibilities for societies to adapt to adverse changes will be radically different, whether the ecohydrological response to changing forces is fast or slow (Hughes *et al* 2013) and whether it is driven by gradual versus critical transitions between states (Scheffer *et al* 2001).

Exploring whether interactions between the hydrological cycle and the vegetation dynamics might explain the recent changes in runoff conditions in the Sahel and involve some potential for tipping is therefore a scientific challenge with a high societal impact. While the existence of bistability and alternative states in semi-arid ecosystems has been investigated either from a conceptual (e.g. Vetter 2005, Turnbull *et al* 2008), observational (e.g. Hirota *et al* 2011, King *et al* 2012, Holmgren *et al* 2013), and modelling (e.g. Kefi *et al* 2010, van Nes *et al* 2014, Cueto-Felgueroso *et al* 2015) perspective, very few studies combined dynamic modelling and observations (e.g. Yin *et al* 2014). We have thus developed a model designed to capture the first-order dynamical interactions (including feedback loops) between the hydrological cycle and the vegetation dynamics in the Sahel, inspired by the work of Scheffer and Carpenter (2003) and van Nes *et al* (2014). The model was tested against data from an experimental site in Mali, with the aim of: (i) demonstrating that it is able to reproduce the observations; (ii) assessing whether the observed evolution might correspond to regime shifts between alternative stable states, triggered by the drought, and (iii) exploring the possible future evolution of the system under climate change and its resilience to rainfall fluctuations.

2. Material and methods

2.1. Study site

The site used in this study is located in northern Mali (Sahel, West Africa), near a place named *Ortonde* (15.15 °N; 1.56 °W), located 20 km from Hombori

Table 1. Mean and standard deviation of the annual precipitation at Hombori for the full period and subperiods.

Periods	Annual precipitation (mm)	
	Mean	sd
1936–2015	374	110
1936–1969 (pre-drought)	421	105
1970–1994 (drought)	325	104
1995–2015 (post-drought)	357	95

village. The climate of the region is semi-arid. The yearly rainfall averages 375 mm over 1936-2015, with rains only occurring between June and September.

The study site is a typical Sahelian banded vegetation pattern also called tiger bush, made of elongated thickets of vegetation perpendicular to the hillslope alternating with runoff-prone bare soil areas (Hiernaux and Gérard 1999). Tiger bush is a natural system encountered in many semi-arid areas over the world (d'Herbés *et al* 2001, Deblauwe *et al* 2008). In this type of ecosystem, the vegetation bands do not produce runoff while intercepting the runoff generated on the upslope bare soil areas. Capture and infiltration of this extra amount of water are essential for the persistence of the vegetation (Ludwig and Tongway 1995, Valentin *et al* 1999, Saco *et al* 2007). Due to low population density, wood cutting and grazing by livestock can be considered negligible on this site, which is also not affected by fires. More details can be found in Trichon *et al* (2018).

Rainfall was measured at the Hombori meteorological station by the Malian Meteorological Service and the AMMA-CATCH Observatory (Galle *et al* 2018). The drought period (1970–1994) resulted in a 100mm deficit (-24%) as compared to the predrought (1936–1969) one (Le Barbe *et al* 2002, Lebel and Ali 2009, Trichon *et al* 2018); the annual rainfall slightly increased from 1995 but remained lower than before the drought (table 1). The inter-annual variability, assessed by the standard deviation of the annual rainfall, remained fairly constant over the different periods (about 95–110 mm y^{-1}). The lag-1 autocorrelation over the full period, equal to 0.45, was used as a measure of the temporal structure of the annual rainfall series.

The evolution of the land cover on the site was assessed by Trichon *et al* (2018), from field surveys over a transect (since 1985), and aerial and satellite images (1955–2015). This dataset describes the evolution of the perennial woody cover, the areas where seasonal herbaceous vegetation can develop, and the runoff-prone bare soil areas (supplementary section S1 available online at stacks.iop.org/ERL/14/105005/mmedia). Those variables evolve over years, with a negligible intra-seasonal cycle. The well-developed woody vegetation bands have progressively shrunk since 1955, especially since the drought. In 1955, the structure of vegetated/bare areas and the near-absence of rills suggested that the thickets completely infiltrated runoff from bare soil patches, and that hillslope-scale runoff was very low, as expected for a healthy tiger bush. A network of rills and gullies progressively developed, leading to a drainage of about 11% and 26% of the site in 1985 and 2015, respectively (Trichon *et al* 2018). These changes show an increase in the interconnection of bare soil patches and of hillslope-scale runoff, although quantitative measurements are lacking. This site is typical of the areas which did not recover after the drought (Gardelle *et al* 2010).

2.2. Model development

The model that was developed describes the main interactions between the land cover and the hydrological cycle for this type of system. It works at a yearly time step and hillslope scale. It is a lumped model, with no dimension in space. Only the main vegetation/hydrology interactions are represented and detailed processes (nutrients/carbon cycle, small-scale erosion, crusting, sediment fluxes...) and their spatial and intra-seasonal variability are implicitly embedded in the lumped model parameters. The two state variables of the model are: (i) the fraction of the surface covered by perennial woody vegetation W (−) and (ii) the runoff-prone bare soil fraction B (−). The remaining fraction H corresponds to areas where annual herbaceous can develop, hence :

$$W + B + H = 1 \quad (1)$$

Thus W and H represent a fraction of the total surface (and not a leaf area); they vary annually and do not have a seasonal cycle. The total W, B and H fractions are simulated without specifying their spatial repartition within the hillslope. The dynamics of each state variable is represented by an ordinary differential equation in time. The annual precipitation P (mm) is the only external force driving the system. In the following, upper case symbols refer to time-varying variables, and lower case symbols to constant parameters.

2.2.1. Water balance

The annual precipitation P (mm) is partitioned into runoff R (mm), which is the net runoff exported out of the system, and $I = P - R$ (mm), which represents the total water available over the year. It is not an actual water storage but an indicator of the soil water amount available for the vegetation during the year; it aggregates evapotranspiration and infiltration.

The hillslope scale runoff coefficient Ke represents the fraction of rainfall P converted to runoff R, which is written:

$$Ke = \frac{R}{P} \quad (2)$$

hence:

$$I = P \cdot (1 - Ke) \quad (3)$$

In the field, the runoff produced locally on bare soil areas can reinfiltrate in herbaceous and woody

Table 2. Variable definitions and ranges of possible values. (*) Assuming recolonization of bare areas is slower than growth in herbaceous areas, we imposed $r_r < r_g$. (**) From Peugeot *et al* (1997) and Galle *et al* (1999).

Symbol	Description	Value	Unit
r_g	Maximum growth rate of woody vegetation in herbaceous zones	]0 ; 1.5]	y^{-1}
r_r	Maximum recolonization rate of woody vegetation in bare soil zones	]0 ; 1.5] (*)	y^{-1}
r_d	Maximum death rate of vegetation	]0 ; 1.5]	y^{-1}
i_g	Half-saturation constant for growth	[250 ; 350]	mm
i_d	Half-saturation constant for death	[100 ; 200]	mm
μ	Spontaneous vegetation growth rate	$[1.10^{-4} ; 1.10^{-3}]$	y^{-1}
α_p	Precipitation efficiency for bare soil growth	$[2.10^{-4} ; 2.10^{-3}]$	$mm^{-1}\,y^{-1}$
α_r	Runoff efficiency for bare soil growth	$[5.10^{-3} ; 5.10^{-2}]$	$mm^{-1}\,y^{-1}$
ke_B	Runoff coefficient of bare soil patches	0.5 (**)	—
l	Connectivity parameter of bare soil patches	[80 ; 220]	—

vegetation patches, but their spatial organization plays a key role: for the same global bare soil fraction B, the runoff at the hillslope scale (hence Ke) is higher if the bare patches are better connected. Following Mayor *et al* (2008), the spatial structure of bare soil patches was parametrized by the flowlength metrics (FL), defined as the mean length of uninterrupted runoff paths along the slope. Rodríguez *et al* (2018) proposed a formulation of FL adapted to the representation of the system on a grid with a known pixel size. Based on their work, we developed a modified formulation of FL which is better adapted to our lumped approach, which writes:

$$FL^* = \frac{2 \cdot B}{l^2 \cdot (1 - B)^2} \cdot (l \cdot (1 - B) - 1 + e^{-l \cdot (1-B)}) \quad (4)$$

where $l(-)$ is a constant parameter representing the effect of the size and spatial organization of patches. FL^* ranges from 0 to 1, and represents the hydrological connectivity along the hillslope (Okin *et al* 2015). The hillslope-scale runoff coefficient Ke (equation (2)) was assumed to be proportional to the flowlength:

$$Ke = ke_B \cdot FL^* \quad (5)$$

where $ke_B(-)$ is the small scale runoff coefficient of bare soil areas.

2.2.2. Woody vegetation dynamics

The dynamics of the perennial woody vegetation W was represented by classical laws used in ecological modelling (van Nes *et al* 2014, Scheffer 2009). It combines four evolution rates representing four dominant processes: (1) growth to the expense of herbaceous zones, (2) recolonization of bare zones, (3) death due to water deficit, and (4) spontaneous growth due to the germination of imported (wind/animal dissemination) or stored seeds. It writes:

$$\frac{dW}{dt} = r_g \cdot \frac{I}{I + i_g} \cdot W \cdot H + r_r \cdot \frac{I}{I + i_r} \cdot W \cdot B - r_d \cdot \frac{i_d}{I + i_d} \cdot W + \mu \quad (6)$$

The meaning of the parameters of this equation are described in table 2, and details on each term are given in supplementary section S2.

2.2.3. Bare soil dynamics

The bare soil fraction B increases at the expense of herbaceous areas H due to crusting and erosion, and decreases due to vegetation expansion. This dynamics is represented by three main processes: (i) increase due to crusting by rainfall (e.g. small-scale splash effect); (ii) increase due to runoff (crusting, erosion); and (iii) decrease due to recolonization by perennial vegetation. For simplicity, we assumed that rainfall and runoff effects on B were proportional to the yearly amounts P and R, and we did not parametrize the effects of rainfall intensities at the event timescale. The dynamics of B writes:

$$\frac{dB}{dt} = H \cdot \alpha_p \cdot P + H \cdot \alpha_r \cdot R - r_r \cdot \frac{I}{I + i_r} \cdot W \cdot B \quad (7)$$

where α_p and α_r are parameters; the rightmost term is identical to equation (S2) (recolonization) and appears in equation (6).

Finally, the model is composed of the differential equations (6) and (7), together with equations (1) to (5).

2.3. Model implementation

The model includes 10 parameters (table 2). The range of l was constrained by fitting equation (4) on flowlength and B values computed on aerial images using the method of Mayor *et al* (2008) (see supplementary section S3). For the others parameters, we defined *a priori* a range of plausible values (table 2).

From these ranges, we built an ensemble of 10^6 sets of parameters using a Latin hypercube sampling method with uniform parameter distributions, with the constraint $r_r \geqslant r_g$. For each parameter set, the model was initialized with W and B observed in 1955 (table S1), and run from 1955 to 2015 using the series of annual rainfall from Hombori. The goodness-of-fit between the simulated and observed time series of W

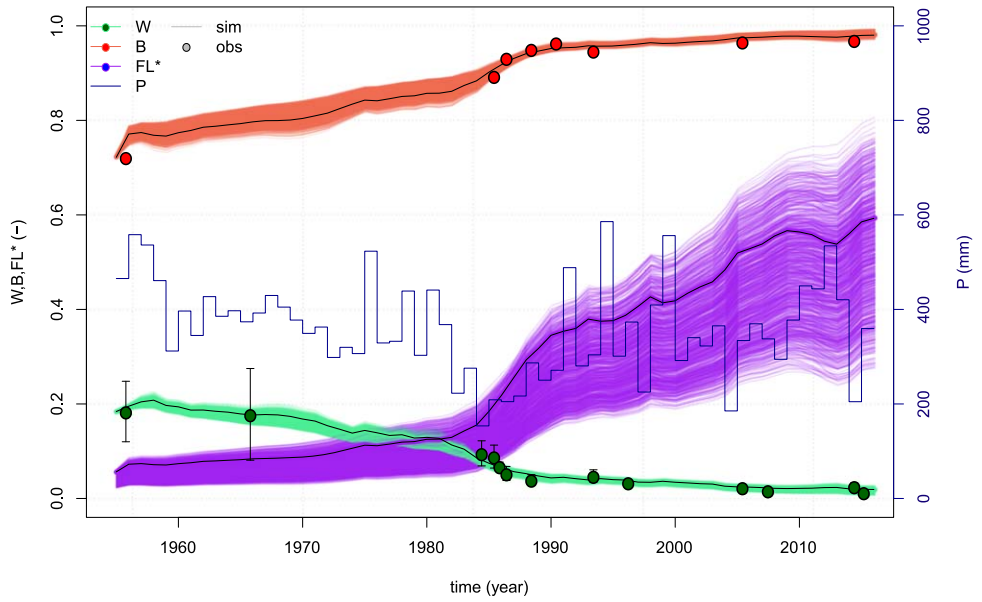

Figure 1. Time series of simulated woody vegetation fraction *W*, bare soil fraction *B* and hydrological connectivity FL^* for the ensemble of 1000 best simulations; black solid line: member with the lowest RMSE; dark blue line: observed rainfall; and circles: observed *W* and *B* fractions.

and *B* (table S1) was estimated by a composite root mean square error (RMSE, see supplementary section S4). The 1000 parameter sets giving the lowest RMSE values were selected as the members of the simulation ensemble. Each member selected by this calibration procedure was considered as an equally plausible model of the system. As estimation errors were not provided for *B* in Trichon *et al* (2018), the calibration was performed without accounting for the uncertainties on *W* and *B*, and the impact of this assumption was evaluated (supplementary section S8).

The model was implemented under the R environment (R/3.4.3), using the 'deSolve' package (Soetaert *et al* 2010) for solving differential equations and 'SAFER' for latin hypercube sampling (Gollini *et al* 2015, Pianosi *et al* 2015). The code was parallelized using the 'parallel' package (R Core Team 2018) and run on a 28-core node on the MESO@LR-Montpellier University computing facility. The simulation of 10^6 sets of parameters over 60 years took ≈2 h on this platform.

2.4. Exploration of the system dynamics

We used the 1000-member simulation ensemble to analyze the properties of the modeled system. For each member, we first determined the equilibrium states for *W*, *B* and *Ke* from the final state reached by the system when forced by long series of constant rainfall (1000 years) with *P* ranging from 150 to 600 mm (supplementary section S5). As the state towards which the system is attracted changes with changing rainfall forcing, the equilibrium states are virtually never reached in the real world. Then, in order to evaluate how rainfall variability determines the system final state (Bathiany *et al* 2018, van der Bolt *et al* 2018), we built a synthetic series of variable rainfall with prescribed statistical properties: mean, standard deviation (*SD*) and lag-1 autocorrelation (*Corr*). *SD* describes the inter-annual variability and *Corr* describes how *P* values are organised in time; high *Corr* values imply longer dry/wet periods. Following Heino *et al* (2000) and Ruokolainen *et al* (2009), we used a red-noise model in which the autocorrelation decreases exponentially as a function of the lag. For a given initial condition and parameter set, the model was forced over 2000 years with the series of synthetic rainfall, exploring a range of mean *P*, *SD* and *Corr*. The response of the system was assessed by the statistical distribution of *W*, *B*, and FL^* over the last 1000 years, to get rid of the influence of the initial condition.

3. Results and discussion

3.1. Model calibration

The 1000-member simulations ensemble reproduced very well the observed evolution of *W* and *B* (figure 1) with a spread lower than the uncertainty on the observations ($RMSE < 0.002\,4$). The flowlength FL^* (proportional to the runoff, equation (5)) was derived from *B* and depends on *l* (equation (4)). The lack of quantitative observations to constrain FL^* (hence *Ke*), the nonlinear dependence between *B* and FL^* (equation (4)) and the additional degree of freedom brought by *l* explains the large spread of FL^* and its increase over time. Despite the spread, the increase of FL^* is consistent with the development of rills and gullies observed on the site (Trichon *et al* 2018).

3.2. Equilibrium states

For all members, the system equilibrates to a degraded state (low *W*, high *B* and FL^*) for $P < 350$ mm, and to

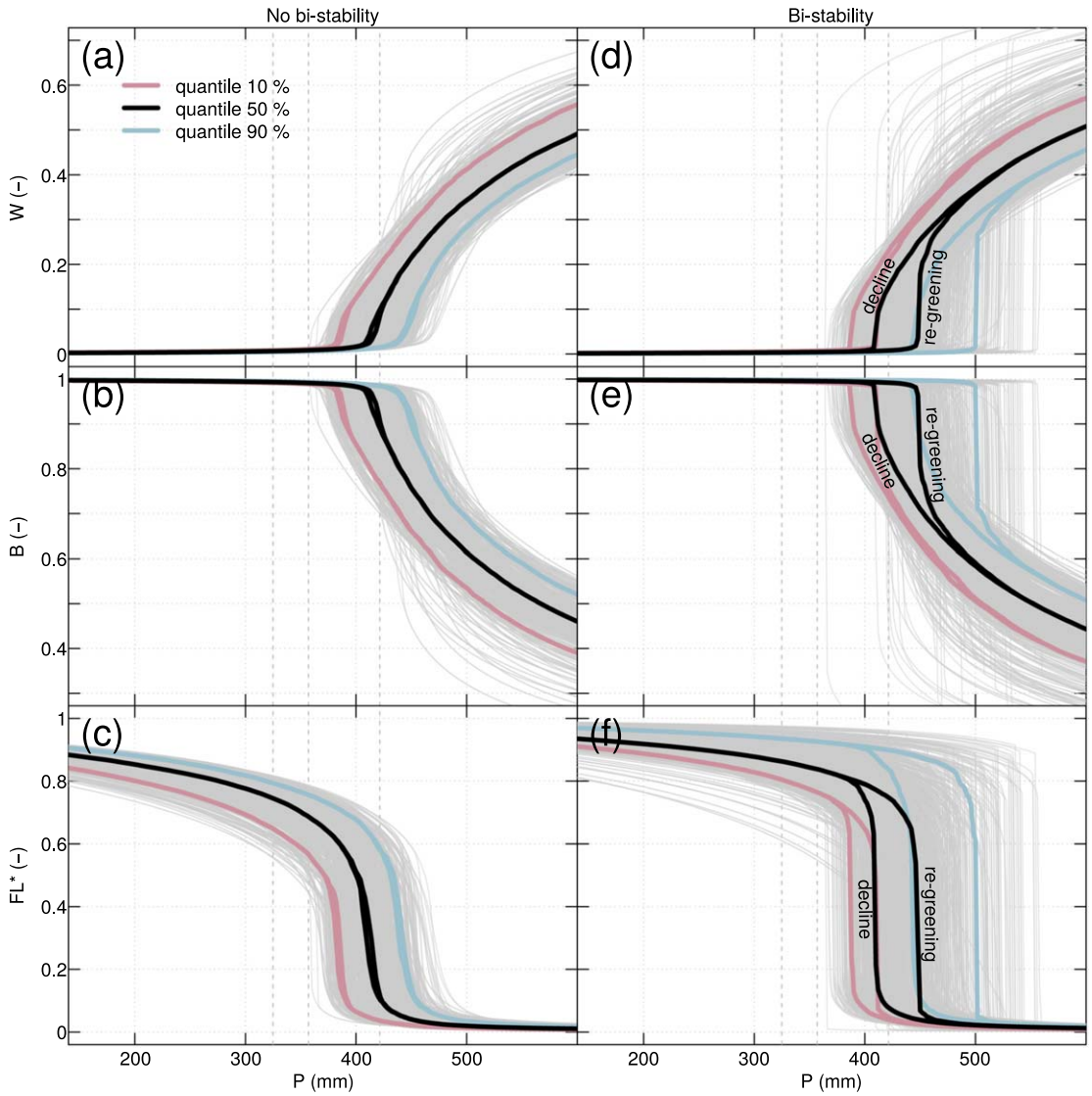

Figure 2. Equilibrium states of woody vegetation fraction W (a), (d), bare soil fraction B (b), (e), and flowlength FL^* (c), (f) versus constant annual rainfall P, for ensemble members without (left column) and with bistability (right column). Quantiles 10, 50 and 90% of the distribution are emphasized (bold lines). For members with bistability (d)–(f), a *decline* and a *regreening* equilibrium coexist over a range of P. Vertical dotted lines represent the mean precipitation for each period of table 1.

a vegetated state for $P > 580$ mm (figure 2). The fraction of woody cover W at equilibrium increases with the rainfall amount, and B and FL^* decrease accordingly. The herbaceous cover fraction H at equilibrium (not shown) is about 0 for the degraded state and ranges from 0.03 to 0.1 for the vegetated one.

For 37% of the members, a single equilibrium state exists (monostability) for each rainfall amount, and the equilibrium value gradually changes with precipitation (figures 2(a)–(c)). For the remaining members (63%), the system is bistable over a range of P values where two equilibria coexist (figures 2(d)–(f)). The bounds of the bistability range correspond to the critical thresholds (tipping points) of the system, which delimit the range of P where the equilibrium state differs depending on whether the system is declining or regreening. The equilibrium curves (figure 2) and the precipitation critical thresholds for mono- and bi-stable members (table 3) are similar along the decline branches, but very different along the regreening ones. Since observations were only available along the decline trajectory of the system, the regreening branches were poorly constrained. Consequently, the value of the critical regreening thresholds and the proportion of bistable members remain uncertain.

Table 3. Annual precipitation thresholds P (mm) for quantiles 10, 50, and 90% of the ensemble members with and without bistability. For monostable cases, the rainfall threshold was defined as the value of P above which a runoff exists ($R > 0.1$).

Quantile	Monostability	Bistability	
		Decline	Regreening
10%	387	390	412
50%	416	412	450
90%	446	446	502

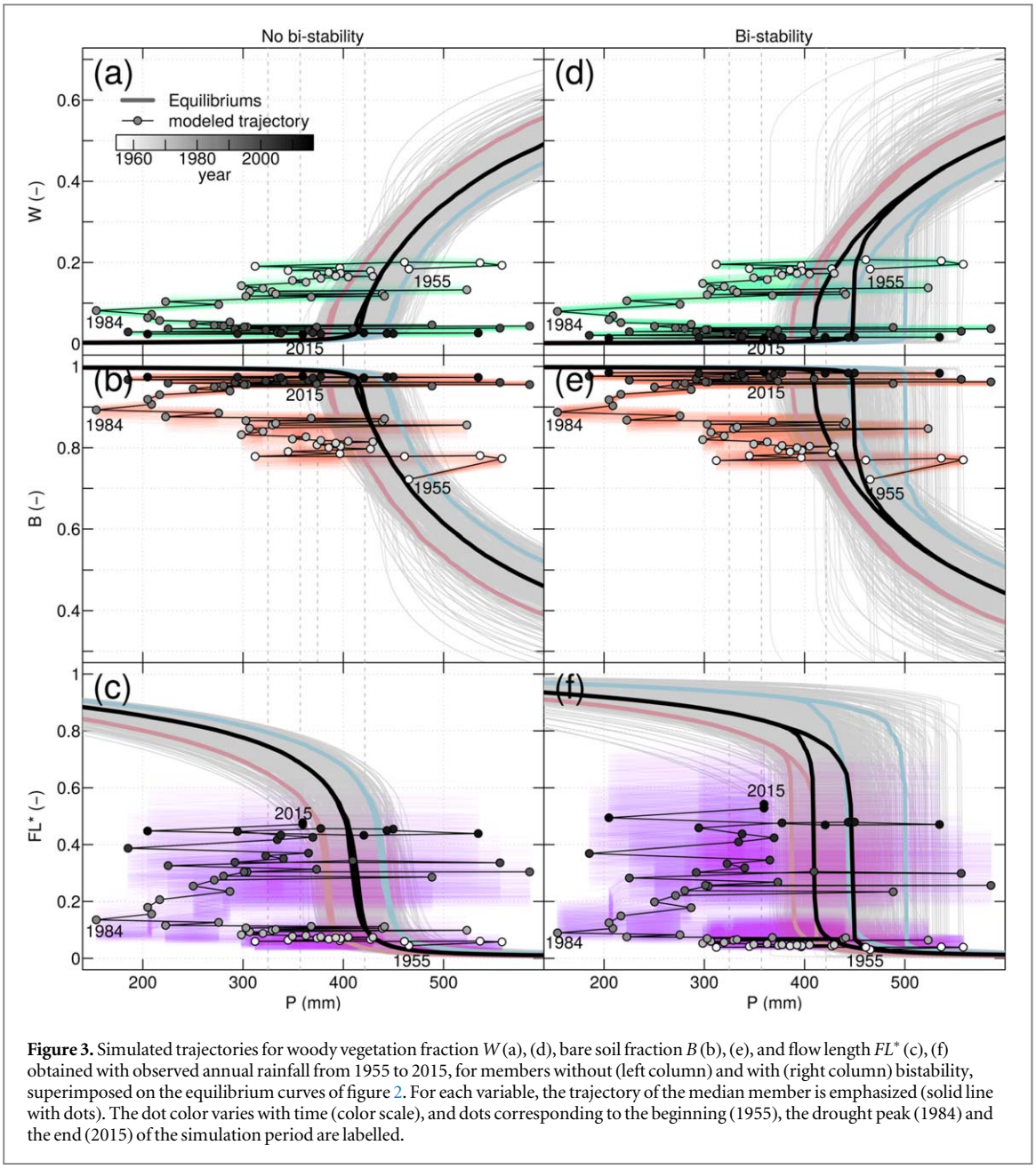

Figure 3. Simulated trajectories for woody vegetation fraction W (a), (d), bare soil fraction B (b), (e), and flow length FL^* (c), (f) obtained with observed annual rainfall from 1955 to 2015, for members without (left column) and with (right column) bistability, superimposed on the equilibrium curves of figure 2. For each variable, the trajectory of the median member is emphasized (solid line with dots). The dot color varies with time (color scale), and dots corresponding to the beginning (1955), the drought peak (1984) and the end (2015) of the simulation period are labelled.

For all members, the degraded state was the only one possible for drought ($P = 325$ mm) and post-drought ($P = 357$ mm) mean precipitation (figure 2). For the pre-drought mean precipitation ($P = 421$ mm), an equilibrium vegetated state with low runoff exists for 73% of the members, of which an alternative degraded equilibrium exists for about one half of them. For the remaining 27%, the attracting equilibrium is the degraded one. All these results were obtained from an ensemble of parameter sets selected without taking into account the uncertainties on the observations, which we could not quantify (section 2.3). We have shown with a sensitivity analysis (supplementary section S8) that accounting for these uncertainties moderately changes the values of the critical thresholds and the proportion of mono- and bi-stable members. Nevertheless, the uncertainties do not affect the qualitative behavior described above and do not call into question the existence of the two alternative stable states, nor the other conclusions of the study.

For most of the members, the system equilibrium is the vegetated/low runoff state before the drought, and the alternative low vegetation/high runoff state since then. However, equilibrium states do not provide information on actual trajectories because the way in which the system converges to these states depends on its evolution rate and on the rainfall variability.

3.3. Actual trajectories

When the model was initialized with the 1955 state and forced with the observed rainfall, all the simulations crossed several times the equilibrium curves during the pre-drought period, oscillating around a vegetated state with $W \approx 0.15$, $B \approx 0.80$ and $FL^* \approx 0.40$ (figure 3). Due to a few very dry years (around 1984) in the drought period, it was pulled far

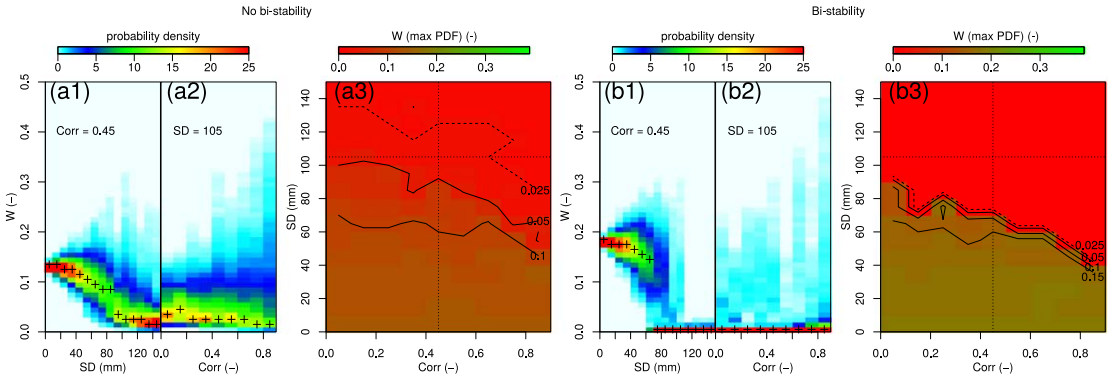

Figure 4. Probability density of woody vegetation fraction W as a function of annual precipitation standard deviation SD and auto-correlation $Corr$ for models initialized with the 1955 conditions and forced by 2000-year synthetic rainfall series with mean $P = 425$ mm. Results for the median member of the ensemble without (a) and with (b) bistability. Probability density of W simulated over the last 1000 years (see methods) as a function of SD for $Corr = 0.45$ (a1), (b1) and of $Corr$ for $SD = 105$ mm (a2), (b2). $SD = 105$ mm and $Corr = 0.45$ were retrieved from the observed rainfall dataset. The crosses in a1, a2, b1, and b2 refer to the maximal probability density of W (mode, the most frequent simulated state). Surface and contour lines of the mode of W in the SD versus $Corr$ space (a3), (b3); the horizontal and vertical dotted lines a3 and b3 locate the observed values $SD = 105$ mm and $Corr = 0.45$.

away from this equilibrium (to the left of the equilibrium curve), while W (resp. B, FL^*) was decreasing (resp. increasing). After the drought, the system remained in a degraded state, despite the occurrence of some wet years ($P > 450$ mm) corresponding to a vegetated equilibrium. Although the range of rainfall variability in every subperiod encompassed P values associated with vegetated and degraded equilibrium, the system did not adjust to them (figure 3), which means that its adjustment timescale is larger than the timescale of rainfall variability.

These results suggest that the drop in the mean annual rainfall between 1970 and 1994 was a major driver of the observed decline of the Ortonde tiger bush. However, the inter-annual variability of rainfall may also have contributed to the destabilization of the system.

3.4. Sensitivity to rainfall variability

Except if the system is extremely slow (insensitive to forcing variability) or extremely reactive (it adjusts immediately to the equilibrium state corresponding to the forcing), the variability of the forcing and its temporal structure can drive oscillations of the system between states (Bathiany *et al* 2018) and trigger critical transitions (van der Bolt *et al* 2018). The sensitivity of the system to rainfall variability was assessed using synthetic annual rainfall series with prescribed mean, standard deviation and lag-1 autocorrelation (section 2.4). This sensitivity is illustrated in figure 4 for the two members corresponding to the median member (supplementary section S6) of the monostable and the bistable simulation subsets, initialized with the 1955 condition.

In the monostable case (figures 4(a1)–(a3)), the distribution of W widens (blue colors) and the mode (most frequent value, crosses) decreases when SD (figure 4(a1)) and $Corr$ (figure 4(a2)) increase: the system gradually shifts from a vegetated to a degraded state when the rainfall variability increases and/or when its temporal structure strengthens (figure 4(a3)). The increased dispersion of W for high values of SD and $Corr$ means that the system can reach a high vegetation states at some time, but it is attracted back to a low W state.

In the bistable case (figures 4(b1)–(b3)), the same type of behaviour is obtained except that beyond a SD threshold ($SD \approx 50$ mm for $Corr = 0.45$ in figure 4(b1)), the distribution of W becomes bimodal ($W \approx 0.15$ and $W \approx 0.01$). For $SD > 80$ mm, the distribution abruptly shrinks and the mode shifts towards $W \approx 0$ (figure 4(b1)). The shift to the degraded state occurs for a lower variability (SD) when $Corr$ increases (figure 4(b3)). It means that due to longer dry and wet periods (high $Corr$), less deviation from the mean rainfall is required to attract the system towards the degraded state (van der Bolt *et al* 2018). In all cases, the system forced with variable precipitation oscillates around a W (resp. B and FL^*) value which is lower (resp. higher) than the equilibrium reached with a constant rainfall ($SD = 0$ on figures 4(a1), (b1)). Increased autocorrelation, which implies longer dry and wet periods, moves the system further from equilibrium during precipitation anomaly periods, which amplifies the effect of the inter-annual variability (figures 4(a3) and 4(b3)). This result can be interpreted by asymmetric declining versus regreening processes: the system degrades more during dry years than it recovers during wet years, which pushes it to a more degraded state when rainfall variability increases.

These results confirm that no vegetated state was possible in both drought and post-drought periods, and that the system remained trapped in the basin of attraction of the degraded state until now. They also show that the reduction of the mean annual rainfall

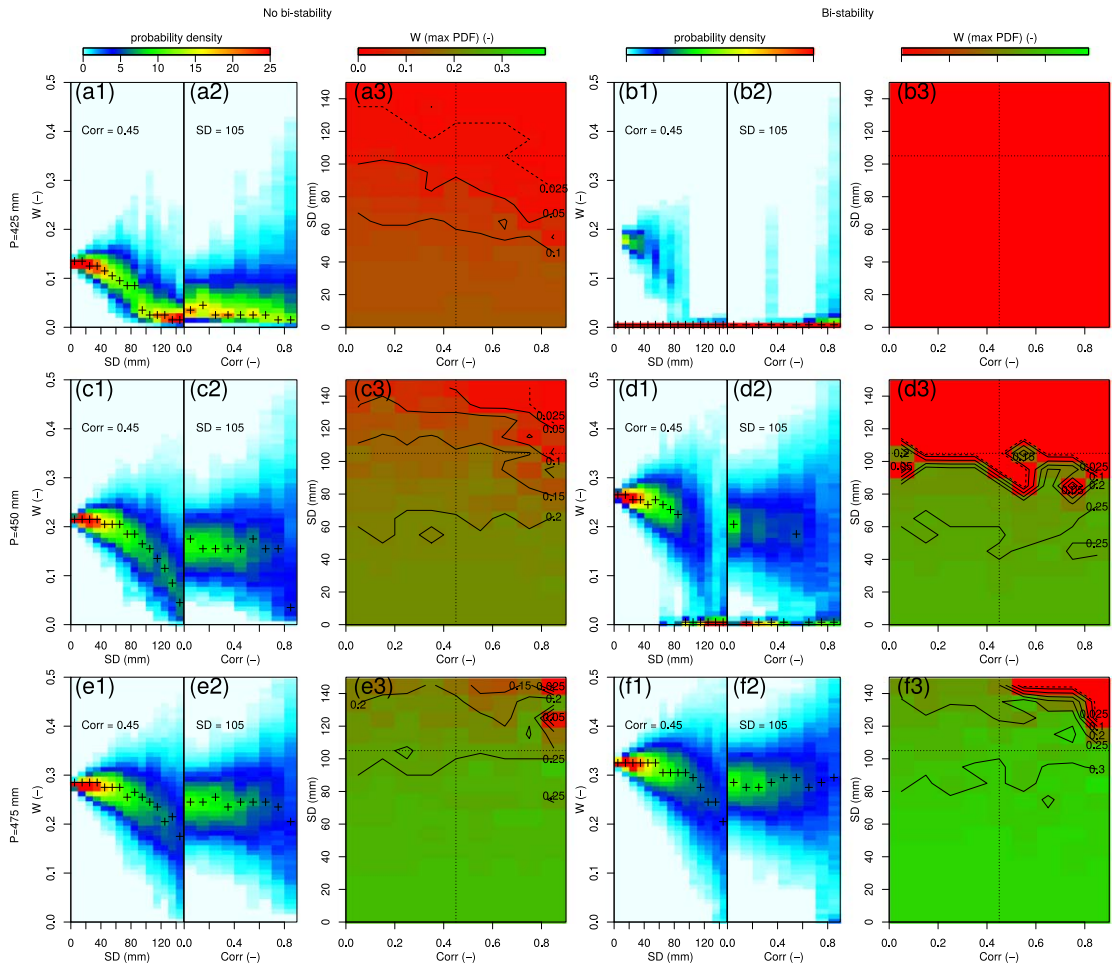

Figure 5. Same as figure 4 for mean annual rainfall $P = 425$ mm (a), (b), $P = 450$ mm (c), (d) and $P = 500$ mm (e), (f), and initialization with the 2014 observed state. The dotted contour line ($W = 0.025$) in (a3)–(f3) corresponds to the initial 2014 condition.

during the drought period is sufficient to explain the observed decline of this tiger bush.

3.5. System resilience

With climate change, the inter-annual variability as well as the length of dry and wet periods may increase in central Sahel in the next decades (Monerie *et al* 2017, Martin 2018). In this region, there is no consensus on the sign of annual precipitation change between global circulation models (Christensen *et al* 2014). Recent studies over the region showed that the annual rainfall may increase in central Sahel (Giannini *et al* 2013, Park *et al* 2016, Monerie *et al* 2017), although this scenario is still uncertain. This trend could bring favourable conditions for the recovery of the Ortonde tiger bush. The resilience of the system, defined as its potential to recover a vegetated state with low runoff, was assessed with the same kind of analysis than in the previous section. The model was initialized with the current state (2014), and forced with synthetic rainfall series with increasing mean rainfall: $P = 425$ mm (≈pre-drought), $P = 450$ mm (+6%), and $P = 475$ mm (+12%), and varying *SD* and *Corr*.

For the median monostable member, the system response to variable rainfall with pre-drought properties is similar to that obtained with the 1955 initial conditions (figures 5(a) and 4(a)), and the current state is stable ($W \approx 0.025$). For higher annual precipitation (figures 5(c), (e)), the system recovers to W values that are larger if P is large, except if both *SD* and *Corr* are high (figures 5(c3) and (e3)).

For the median bistable member, the system remains on the degraded state for pre-drought mean precipitation, with little fluctuations (figure 5(b)), whereas a vegetated state exists with the 1955 initial condition (figure 4(b)). This difference underlines the effect of the bi-stability: with the 2014 initial condition, the system lies in the basin of attraction of the degraded state, whereas it is attracted by the alternative vegetated state with the 1955 condition. For $P = 450$ mm, the system is bi-stable for $50\text{ mm} < SD < 130\text{ mm}$ ($Corr = 0.45$). Bi-stability almost disappears for $P = 475$ mm, and the system recovers except when $SD \geqslant 110$ mm and $Corr \geqslant 0.5$ (figure 5(f)). Along with vegetation recovery, the model simulates a reduction of the runoff capacity (supplementary section S7), associated with the reduction of bare soil areas. However, the rills and gullies

that developed on the site will hardly disappear. These durable physical changes imply that the system cannot recover following the same pathway back. As such changes in the hydrological structure are not represented in our model, our results could overestimate the resilience of the system.

For all members the shift between states occurs for higher mean precipitation when the rainfall variability (SD and/or Corr) increases, e.g. the iso-value $W = 0.05$ moves to domains with higher *SD* and *Corr* when *P* increases (figures 5(a3)–(c3)–(e3), and (d3)–(f3)). It implies that under variable precipitation forcing, the regime shift will occur for higher precipitation values than assessed from constant rainfall (table 3 and figure 2).

According to the model, a regreening of the system from its current state is possible. It requires the mean annual precipitation to be at least equal to its pre-drought value ($P \approx 425$ mm) which is sufficient if the rainfall variability is low and if the system is not bistable. If the system is bistable, a higher mean precipitation is required, at least equal to the regreening critical threshold for constant rainfall (figure 2 and table 3). This value is not sufficient considering annual rainfall variability, as illustrated in figure 5(d3) for the median, bistable member: with the current rainfall variability ($SD = 105$ mm, $Corr = 0.45$), $P = 450$ mm is no longer sufficient for regreening, whereas it is the regreening threshold in table 3.

Considering the future rainfall increase as a working assumption, we have estimated from Monerie *et al* (2017) that the mean annual precipitation may reach about 475 mm by the end of the 21st century in Northern Mali. Similarly, the rainfall variability may increase, with an estimated *SD* increment of about 50 mm. Thus, according to our simulations, the simultaneous increase in annual totals and interannual rainfall variability would lead to antagonistic effects on the resilience of the system and, therefore, an uncertain future. The red noise model used to assess the effect of rainfall variability poorly represents the strong decadal structure of Sahelian rainfall (Dieppois *et al* 2013), and the effect of the temporal structure of rainfall may be stronger than estimated. Furthermore, a larger intraseasonal variability is also anticipated in a warmer climate (Martin 2018), which could also affect the potential for resilience.

In addition to the intraseasonal rainfall variability and the hydrological effects of rills, other factors such as air temperature have been omitted in our simple model. We used rainfall as unique forcing because vegetation and runoff changes were more driven by rainfall than temperature changes over the past decades (Hiernaux *et al* 2009, 2009, Leauthaud *et al* 2017). Temperature increase is a robust trend globally (Christensen *et al* 2014), it and could play a major eco-hydrological role in the future. Increased temperature-controlled evaporation may increase the water stress (Young *et al* 2017). However the effects of higher temperature on the physiology of tropical plants are largely unknown and deserve specific studies (Jones 1992, Cavaleri *et al* 2015). Although direct and indirect temperature effects are uncertain, it is probable that higher temperature will reduce rather than improve the future resilience of Sahelian ecosystems.

4. Conclusions and prospects

We developed a system dynamics model to represent the ecohydrological evolution of a Sahelian tiger bush over decades, constrained by observation data. The model represents the first order interactions (including retroactions) between hydrology and vegetation. Although based on a simple representation of the studied tiger bush, the model was able to reproduce the observed vegetation decline and the associated increase in surface runoff over the 1955–2015 period. Based on field work, these trends are robust and are iconic of the declining systems in the region. According to our simulations, the system was oscillating around a vegetated state before the 1970–94 drought, as a response to rainfall variability. Then it started to shift to a degraded (low vegetation/high runoff) state around which it currently remains, despite a slight rainfall recovery. We have confirmed that this decline corresponds to a shift between two stable states: a vegetated/low runoff state and a low vegetation/high runoff state. The drop in the mean annual precipitation associated with the drought was found to be sufficient to explain this regime shift. We could not conclude whether the shift occurred as a gradual response to the changing forcing or if it implied critical transitions (hence bistability), both modalities of change being plausible in our simulation ensemble.

We showed that increased variability in annual rainfall (amplitude of variation and temporal structure) pushes the system towards more degraded states. Rainfall increase in central Sahel is a possible trend anticipated in some climate change scenarios, but its effect on vegetation recovery may be offset by the concurrent increase expected in rainfall variability. According to our simulations, the Sahelian tiger bush is resilient. However, as the model was only constrained along the decline trajectory observed on a particular site, the critical rainfall conditions for resilience could not be evaluated precisely. Moreover, the simple model structure and some unaccounted processes (impacts of higher temperature, effect of gullies) might well lead to over-estimate the resilience of the system. Our study has yielded robust qualitative conclusions on the existence of alternative stable states in such systems and on their resilience potential, but due to the remaining uncertainties we could not make quantitative predictions.

The main conclusion of this study is that a drought-induced regime shift can explain the runoff increase observed at the hillslope-scale in some Sahelien landscapes. In a future work, the model will be applied to various sites representative of the diversity of Sahelian ecohydrosystems, including regreening ones (Dardel *et al* 2014). This will quantify the role of hillslope-scale regime shifts in the concurrent regreening and runoff increase trends observed at the regional scale.

Acknowledgments

This study was funded by IRD through a post-doctoral fellowship contract. It has been realized with the support of the High Performance Computing Platform MESO@LR, financed by the Occitanie/Pyrénées-Méditerranée Region, Montpellier Mediterranean Metropole and the University of Montpellier (France). The authors are grateful to the Malian Meteorological Service for the historical rainfall datasets. Recent observations were provided by the AMMA-CATCH observatory www.amma-catch.org. The authors thank V Dakos and S Kéfi for fruitful discussions about this work, and the two anonymous reviewers for their input, which improved the manuscript.

Data availability statements

The data that support the findings of this study are presented in Trichon *et al* (2018). The land cover dataset, derived from Trichon *et al* (2018), is given in supplementary section S1 (table S1). The yearly rainfall series at the Hombori meteorological station, from the Malian Meteorological Service and the AMMA-CATCH Observatory (Galle *et al* 2018), is not publicly available for legal reasons, but it is available from the corresponding author upon reasonable request.

ORCID iDs

Valentin Wendling https://orcid.org/0000-0003-4163-9700
Christophe Peugeot https://orcid.org/0000-0003-2161-125X
Angeles G Mayor https://orcid.org/0000-0001-8097-5315
Pierre Hiernaux https://orcid.org/0000-0002-1764-9178
Eric Mougin https://orcid.org/0000-0002-7569-5906
Manuela Grippa https://orcid.org/0000-0002-4889-7975
Laurent Kergoat https://orcid.org/0000-0003-1792-8473
Romain Walcker https://orcid.org/0000-0002-5769-810X
Sylvie Galle https://orcid.org/0000-0002-3100-8510
Thierry Lebel https://orcid.org/0000-0002-1297-6751

References

Barnosky A D *et al* 2012 *Nature* **486** 52–8
Bathiany S, Scheffer M, Nes E H V, Williamson M S and Lenton T M 2018 *Sci. Rep.* **8** 5040
Broderstad E G and Eythorsson E 2014 *Ecol. Soc.* **19** 1
Brook B W, Ellis E C, Perring M P, Mackay A W and Blomqvist L 2013 *Trends Ecol. Evol.* **28** 396–401
Casenave A and Valentin C 1992 *J. Hydrol.* **130** 231–49
Cavaleri M A, Reed S C, Smith W K and Wood T E 2015 *Global Change Biol.* **21** 2111–21
Christensen J *et al* 2014 2013: Climate phenomena and their relevance for future regional climate change *Climate Change 2013: The Physical Science Basis. Contribution of Working Group I to the Fifth Assessment Report of the Intergovernmental Panel on Climate Change* ed T F Stocker *et al* (Cambridge: Cambridge University Press) pp 1217–308
Claussen M, Kubatzki C, Brovkin V, Ganopolski A, Hoelzmann P and Pachur H J 1999 *Geophys. Res. Lett.* **26** 2037–40
Cueto-Felgueroso L, Dentz M and Juanes R 2015 *Phys. Rev.* E **91** 052148
Dardel C, Kergoat L, Hiernaux P, Grippa M, Mougin E, Ciais P and Nguyen C C 2014 *Remote Sensing* **6** 3446–74
Dardel C, Kergoat L, Hiernaux P, Mougin E, Grippa M and Tucker C 2014 *Remote Sens. Environ.* **140** 350–64
Deblauwe V, Barbier N, Couteron P, Lejeune O and Bogaert J 2008 *Global Ecol. Biogeogr.* **17** 715–23
Descroix L, Genthon P, Amogu O, Rajot J L, Sighomnou D and Vauclin M 2012 *Global Planet. Change* **98-99** 18–30
Descroix L *et al* 2018 *Water* **10** 748
d'Herbés J M, Valentin C, Tongway D J and Leprun J C 2001 *Banded Vegetation Patterning in Arid and Semiarid Environments: Ecological Processes and Consequences for Management* ed D J Tongway, C Valentin and J Seghieri (New York: Ecological Studies Springer) pp 1–19
Di Baldassarre G, Viglione A, Carr G, Kuil L, Salinas J L and Blöschl G 2013 *Hydrol. Earth Syst. Sci.* **17** 3295–303
Dieppois B, Diedhiou A, Durand A, Fournier M, Massei N, Sebag D, Xue Y and Fontaine B 2013 *J. Geophys. Res.: Atmos.* **118** 12587–99
D'Odorico P, Bhattachan A, Davis K F, Ravi S and Runyan C W 2013 *Adv. Water Res.* **51** 326–44
Downey S S, Haas W R and Shennan S J 2016 *Proc. Natl Acad. Sci.* **113** 9751–6
Favreau G, Cappelaere B, Massuel S, Leblanc M, Boucher M, Boulain N and Leduc C 2009 *Water Resour. Res.* **45** W00A16
Fensholt R *et al* 2012 *Remote Sens. Environ.* **121** 144–58
Gal L, Grippa M, Hiernaux P, Peugeot C, Mougin E and Kergoat L 2016 *J. Hydrol.* **540** 1176–88
Gal L, Grippa M, Hiernaux P, Pons L and Kergoat L 2017 *Hydrol. Earth Syst. Sci.* **21** 4591–613
Galle S, Ehrmann M and Peugeot C 1999 *CATENA* **37** 197–216
Galle S *et al* 2018 *Vadose Zone J.* **17** 180062
Gardelle J, Hiernaux P, Kergoat L and Grippa M 2010 *Hydrol. Earth Syst. Sci.* **14** 309–24
Giannini A, Salack S, Lodoun T, Ali A, Gaye A T and Ndiaye O 2013 *Environ. Res. Lett.* **8** 024010
Gollini I, Pianosi F, Sarrazin F and Wagener T 2015 SAFER: Sensitivity Analysis For Everybody with R. R package version 1.1 (http://bristol.ac.uk/cabot/resources/safe-toolbox/)
Heino M, Ripa J and Kaitala V 2000 *Ecography* **23** 177–84
Hiernaux P, Ayantunde A, Kalilou A, Mougin E, Gérard B, Baup F, Grippa M and Djaby B 2009 *J. Hydrol.* **375** 65–77
Hiernaux P, Diarra L, Trichon V, Mougin E, Soumaguel N and Baup F 2009 *J. Hydrol.* **375** 103–13

Hiernaux P and Gérard B 1999 *Acta Oecologica* **20** 147–58
Hiernaux P, Mougin E, Diarra L, Soumaguel N, Lavenu F, Tracol Y and Diawara M 2009 *J. Hydrol.* **375** 114–27
Hirota M, Holmgren M, Nes E H V and Scheffer M 2011 *Science* **334** 232–5
Holmgren M, Hirota M, van Nes E H and Scheffer M 2013 *Nat. Clim. Change* **3** 755–8
Hughes T P, Carpenter S, Rockström J, Scheffer M and Walker B 2013 *Trends Ecol. Evol.* **28** 389–95
Hughes T P, Linares C, Dakos V, van de Leemput I A and van Nes E H 2013 *Trends Ecol. Evol.* **28** 149–55
Jones H G 1992 *Plants and Microclimate: A Quantitative Approach to Environmental Plant Physiology* (Cambridge: Cambridge University Press)
Kefi S, Eppinga M B, de Ruiter P C and Rietkerk M 2010 *Theor. Ecol.* **3** 257–69
Kefi S, Holmgren M and Scheffer M 2016 *Funct. Ecol.* **30** 88–97
King E G, Franz T E and Caylor K K 2012 *Ecohydrol.* **5** 733–45
Kuil L, Carr G, Viglione A, Prskawetz A and Blöschl G 2016 *Water Resour. Res.* **52** 6222–42
Le Barbe L, Lebel T and Tapsoba D 2002 *J. Clim.* **15** 187–202
Leauthaud C *et al* 2017 *Int. J. Climatol.* **37** 2699–718
Lebel T and Ali A 2009 *J. Hydrol.* **375** 52–64
Lenton T M, Held H, Kriegler E, Hall J W, Lucht W, Rahmstorf S and Schellnhuber H J 2008 PNAS **105** 1786–93
Ludwig J A and Tongway D J 1995 *Landscape Ecology* **10** 51–63
Mahé G and Paturel J E 2009 *C.R. Geosci.* **341** 538–46
Martin E R 2018 *Geophys. Res. Lett.* **45** 11913–20
Mayor A G, Bautista S, Small E E, Dixon M and Bellot J 2008 *Water Resour. Res.* **44** W10423
Mayor A G, Kéfi S, Bautista S, Rodríguez F, Cartení F and Rietkerk M 2013 *Landscape Ecology* **28** 931–42
Monerie P A, Sanchez-Gomez E, Pohl B, Robson J and Dong B 2017 *Environ. Res. Lett.* **12** 114003
Okin G S, Heras M M D L, Saco P M, Throop H L, Vivoni E R, Parsons A J, Wainwright J and Peters D P 2015 *Frontiers in Ecology and the Environment* **13** 20–7
Panthou G, Lebel T, Vischel T, Quantin G, Sane Y, Ba A, Ndiaye O, Diongue-Niang A and Diopkane M 2018 *Environ. Res. Lett.* **13** 064013
Park J Y, Bader J and Matei D 2016 *Nature Clim. Change* **6** 941–5
Peugeot C, Esteves M, Galle S, Rajot J L and Vandervaere J P 1997 *J. Hydrol.* **188-189** 179–202
Pianosi F, Sarrazin F and Wagener T 2015 *Environ. Modelling Softw.* **70** 80–5
R Core Team 2018 *R: A Language and Environment for Statistical Computing* (Austria: R Foundation for Statistical Computing Vienna)
Rietkerk M, Dekker S C, Ruiter P C D and Koppel J V D 2004 *Science* **305** 1926–9
Rodríguez F, Mayor A G, Rietkerk M and Bautista S 2018 *Ecol. Indic.* **94** 512–9
Ruokolainen L, Lindén A, Kaitala V and Fowler M S 2009 *Trends Ecol. Evol.* **24** 555–63
Saco P M, Moreno-de las Heras M, Keesstra S, Baartman J, Yetemen O and Rodríguez J F 2018 *Current Opinion in Environmental Science & Health* **5** 67–72
Saco P M, Willgoose G R and Hancock G R 2007 *Hydrol. Earth Syst. Sci.* **11** 1717–30
Scheffer M 2009 *Critical Transitions in Nature and Society* (Princeton, NJ: Princeton University Press)
Scheffer M, Carpenter S, Foley J A, Folke C and Walker B 2001 *Nature* **413** 591
Scheffer M and Carpenter S R 2003 *Trends Ecol. Evol.* **18** 648–56
Sivapalan M 2015 *Water Resour. Res.* **51** 4795–805
Soetaert K, Petzoldt T and Setzer R W 2010 *J. Stat. Software* **33** 1–25
Staver A C, Archibald S and Levin S 2011 *Ecology* **92** 1063–72
Steffen W *et al* 2018 *Proc. Natl Acad. Sci.* **115** 8252–9
Tamagnone P, Massazza G, Pezzoli A and Rosso M 2019 *Water* **11** 156
Taylor C M, Belušić D, Guichard F, Parker D J, Vischel T, Bock O, Harris P P, Janicot S, Klein C and Panthou G 2017 *Nature* **544** 475–8
Trichon V, Hiernaux P, Walcker R and Mougin E 2018 *Global Change Biol.* **24** 2633–48
Turnbull L, Wainwright J and Brazier R E 2008 *Ecohydrology* **1** 23–34
UN 2017 World population prospects. the 2017 revision. key findings and advance tables Technical Report ESA/P/WP/248 United Nations, Department of Economic and Social Affairs, Population division
Valentin C, d'Herbès J M and Poesen J 1999 *CATENA* **37** 1–24
van der Bolt B, van Nes E H, Bathiany S, Vollebregt M E and Scheffer M 2018 *Nat. Clim. Change* **8** 478–84
van Nes E H, Hirota M, Holmgren M and Scheffer M 2014 *Global Change Biol.* **20** 1016–21
Vetter S 2005 *J. Arid. Environ.* **62** 321–41
Wilcox B P, Le Maitre D, Jobbagy E, Wang L and Breshears D D 2017 *Rangeland Systems: Processes, Management and Challenges* ed D D Briske (Cham: Springer) pp 85–129
Wilcox C, Vischel T, Panthou G, Bodian A, Blanchet J, Descroix L, Quantin G, Cassé C, Tanimoun B and Kone S 2018 *J. Hydrol.* **566** 531–45
Yin Z, Dekker S C, van den Hurk B J J M and Dijkstra H A 2014 *Earth Sys. Dyn.* **5** 257–70
Young D J N, Stevens J T, Earles J M, Moore J, Ellis A, Jirka A L and Latimer A M 2017 *Ecol. Lett.* **20** 78–86